

Inferring High-Order Couplings with Neural Networks

Aurélien Decelle and Beatriz Seoane

Departamento de Física Teórica, Universidad Complutense de Madrid, 28040 Madrid, Spain and
Université Paris-Saclay, CNRS, INRIA Tau team, LISN, 91190 Gif-sur-Yvette, France

Alfonso de Jesús Navas Gómez*

Departamento de Física Teórica, Universidad Complutense de Madrid, 28040 Madrid, Spain

Maximum-entropy methods, rooted in the inverse Ising/Potts problem from statistical mechanics, have become indispensable tools for modeling pairwise interactions in disciplines such as bioinformatics, ecology, and neuroscience. Despite their remarkable success, these methods often overlook high-order interactions that may be crucial in complex systems. Conversely, while modern machine learning approaches can capture such interactions, existing interpretable frameworks are computationally expensive, making it impractical to assess the relevance of high-order interactions in real-world scenarios. Restricted Boltzmann Machines (RBMs) offer a computationally efficient alternative by encoding statistical correlations via hidden nodes in a bipartite neural network. Here, we present a method that maps RBMs exactly onto generalized Potts models with interactions of arbitrary high order. This approach leverages large- N approximations, facilitated by the simple architecture of the RBM, to enable the efficient extraction of effective many-body couplings with minimal computational cost. This mapping also enables the development of a general formal framework for the extraction of effective higher-order interactions in arbitrarily complex probabilistic models. Additionally, we introduce a robust formalism for gauge fixing within the generalized Potts model. We validate our method by accurately recovering two- and three-body interactions from synthetic datasets. Additionally, applying our framework to protein sequence data demonstrates its effectiveness in reconstructing protein contact maps, achieving performance comparable to state-of-the-art inverse Potts models. These results position RBMs as a powerful and efficient tool for investigating high-order interactions in complex systems.

Introduction.— The Maximum Entropy (ME) principle in data-driven modeling consists of fitting empirical low-order moments of the data, such as means and covariances, while making minimal assumptions about unobserved variables. In the case of network inference with categorical variables, ME data modeling poses an inverse Potts problem of statistical mechanics, i.e., we seek the fields and pairwise couplings of a magnetic Potts Hamiltonian that best describes the observed data. This approach is interpretable and parsimonious, keeping overfitting under control even with limited data. It has provided a framework for understanding the underlying dynamics of many complex systems [1], including neural circuits [2–5], gene networks [6, 7], protein structures [8–10], collective behaviors, and ecosystems [11]. However, the expressiveness of pairwise models is inherently limited, as they reduce all group interactions to pairwise terms, failing to capture the higher-order interactions crucial in real-world systems [12]. On the other hand, modern generative machine learning models have achieved remarkable breakthroughs recently, such as predicting protein structures from sequences [13, 14]. Nevertheless, state-of-the-art methods often struggle in data-short scenarios and lack of interpretability, making extracting meaningful and understandable insights from their parameters challenging. However, efforts to address these limitations are ongoing [15, 16].

An alternative that effectively mediates between simple pairwise modeling and modern deep learning frameworks is the Restricted Boltzmann Machine (RBM) [17]. In contrast to traditional pairwise models, an RBM works on a bipartite graph in which only one layer embodies the observable data. The introduction of latent or hidden variables gives RBMs the ability to act as universal approximators [18]. This property significantly increases their expressive power while keeping the number of parameters to be learned under control. Recent studies have shown that binary RBMs can be reinterpreted as a generalized Ising or lattice gas model with interactions that go beyond pairwise to include higher-order terms [19–22]. Such a mapping has proven to be useful for inference applications as they allowed the extraction of coupling parameters from simulated data with multi-body interactions requiring equal or fewer parameters than analogous inverse Ising models [22]. This underscores the superior capability of RBMs to model complex systems, offering enhanced performance over standard ME techniques without incurring additional computational costs.

Most applications of ME focus on categorical variables rather than binary ones. A prominent example is Direct Coupling Analysis (DCA), which uses inverse Potts models to infer epistatic couplings from the Multiple Sequence Alignment (MSA) of protein or RNA families [8, 23]. MSAs align sequences from homologous families—groups of proteins or RNAs with a common evolutionary ancestor—to identify conserved regions, revealing structural,

* alfonn01@ucm.es

functional, and evolutionary relationships. Recent studies introduced methods to identify the closest pairwise model distribution to a trained probabilistic model, enabling the extraction of effective pairwise couplings from neural networks [15, 24]. However, these approaches are computationally intensive, requiring either averaging over numerous single-site data permutations or performing sampling, which limits their applicability to pairwise interactions. In this work, we extend these methods to infer n -th order couplings from generic probabilistic models and propose a fast, reliable framework to approximate high-order couplings in RBMs by exploiting their simple energy function structure. We show that the derived expressions accurately infer pairwise and three-wise couplings in controlled experiments and enable protein contact predictions from trained RBMs with accuracy comparable to state-of-the-art DCA methods.

The Potts-Bernoulli RBM.— Consider an undirected stochastic neural network defined on a bipartite lattice, a visible layer $\mathbf{v} = \{v_i\}_{i=1}^{N_v}$, which represents the data, and a hidden layer $\mathbf{h} = \{h_a\}_{a=1}^{N_h}$, which encodes the interactions among the visible variables. As in other energy-based generative models, the joint probability of any given configuration $\{\mathbf{v}, \mathbf{h}\}$ is given by the Boltzmann distribution

$$p(\mathbf{v}, \mathbf{h}) = \frac{1}{Z} e^{-\mathcal{H}(\mathbf{v}, \mathbf{h})}, \text{ where } Z = \sum_{\{\mathbf{v}, \mathbf{h}\}} e^{-\mathcal{H}(\mathbf{v}, \mathbf{h})}, \quad (1)$$

with $\mathcal{H}(\mathbf{v}, \mathbf{h})$ being the *energy function* or the *Hamiltonian* of the model. We define the hidden nodes as Bernoulli variables, i.e., $h_a \in \{0, 1\}$, and the visible nodes as categorical variables, or Potts “spins”, that can take on q states or colors, i.e., $v_i \in \{1, \dots, q\}$. Hence, the Hamiltonian of such a system is given by

$$\mathcal{H}(\mathbf{v}, \mathbf{h}) = - \sum_{i, a, \mu} W_{ia}^\mu h_a \delta_\mu^{v_i} - \sum_{i, \mu} b_i^\mu \delta_\mu^{v_i} - \sum_a c_a h_a, \quad (2)$$

where δ_i^j denote the Kronecker delta ($\delta_i^j = 1$ if $i = j$, and $\delta_i^j = 0$ otherwise), and $\Theta \equiv \{\mathbf{W}, \mathbf{b}, \mathbf{c}\}$ are the model parameters. The *weight tensor* $\mathbf{W} = \{W_{ia}^\mu\}$, is a rank-3 tensor that models the interactions between the visible and hidden layers, and the *visible* and *hidden biases*, denoted by $\mathbf{b} = \{b_i^\mu\}$ and $\mathbf{c} = \{c_a\}$, respectively, are local fields acting in a specific visible or hidden site in the lattice. For clarity, we use Latin indexes $i \in \{1, \dots, N_v\}$ and $a \in \{1, \dots, N_h\}$ to denote visible and hidden sites, respectively, and Greek ones $\mu \in \{1, \dots, q\}$ to indicate the possible colors of the visible variables.

The RBM parameters are usually trained through likelihood maximization to ensure that the marginal distribution on the visible units, $p(\mathbf{v}) = \sum_{\mathbf{h}} p(\mathbf{v}, \mathbf{h})$, closely approximates the empirical distribution of the dataset. See Sect. A in the Appendix for training details.

It is easy to verify that the parameter transformation

$$W_{ia}^\mu \rightarrow W_{ia}^\mu + A_{ia}, \quad b_i^\mu \rightarrow b_i^\mu + B_i, \quad c_a \rightarrow c_a - \sum_i A_{ia}$$

leaves the Boltzmann distribution in (1) unchanged. Such invariance is a natural consequence of the over-parametrization of Potts models [8, 24]. Fixing the model gauge is helpful to uniquely define the inference problem and ensure efficient convergence to optimal parameters during training. The most widely used gauges are the *lattice gas* gauge, which assumes

$$b_i^q = W_{ia}^q = 0, \quad \forall i, a, \quad (3)$$

and the *zero-sum* gauge, defined by

$$\sum_\mu \hat{b}_i^\mu = \sum_\mu \hat{W}_{ia}^\mu = 0, \quad \forall i, a. \quad (4)$$

Hereafter, we will use the “ $\hat{\cdot}$ ” (hat) symbol to refer to the couplings in their correspondingly zero-sum gauge. We did not observe any particular advantage or disadvantage in using either gauge during RBM training. For consistency, we employed the zero-sum gauge during the RBM training analyzed in our experiments.

Generalized multi-body Potts model.— The binary RBM is a universal approximator [18], capable of modeling any multivariate random variable over a binary vector space given sufficient hidden units. Thus, when the dataset comprises equilibrium configurations of a multi-body Ising Hamiltonian, RBM learning can capture interactions of any order among visible units, provided enough data is available. This theoretical property has been demonstrated in practice: recent studies [19–22] have shown that the energy function of a binary RBM can be precisely mapped to an effective Ising model with interactions of all orders, represented by coupling tensors dependent on the RBM parameters Θ . Ref. [22] demonstrated that this mapping can accurately reconstruct the underlying interactions, including three-body terms, through controlled inverse experiments. This work extends the previous mapping to any categorical RBM, focusing on transforming the marginal Hamiltonian of the Potts-Bernoulli RBM,

$$\mathcal{H}(\mathbf{v}) = - \sum_{i, \mu} b_i^\mu \delta_\mu^{v_i} - \sum_a \ln \left(1 + e^{c_a + \sum_{i, \mu} W_{ia}^\mu \delta_\mu^{v_i}} \right), \quad (5)$$

into a generalized Potts Hamiltonian with multi-body interactions,

$$\mathcal{H}(\mathbf{v}) = - \sum_{i, \mu} H_i^\mu \delta_\mu^{v_i} - \sum_{1 \leq i_1 < i_2 \leq N_v} \sum_{\mu_1, \mu_2} J_{i_1 i_2}^{\mu_1 \mu_2} \delta_{\mu_1}^{v_{i_1}} \delta_{\mu_2}^{v_{i_2}} + \dots \quad (6)$$

The goal is to derive explicit expressions for the fields H_i^μ and n -th order couplings $J_{i_1 \dots i_n}^{\mu_1 \dots \mu_n}$ in terms of Θ , providing a physical interpretation of the learned model.

We note that model (6) needs gauge fixing, just as we did with the Potts-Bernoulli Hamiltonian in (2). In this case, the lattice-gas gauge condition is

$$H_i^q = J_{i_1 i_2}^{\mu_1 q} = \dots = J_{i_1 \dots i_{N_v}}^{\mu_1 \dots q} = 0, \quad (7)$$

while that of the zero-sum gauge is

$$\sum_{\mu'} \hat{H}_i^{\mu'} = \sum_{\mu'} J_{i_1 i_2}^{\mu_1 \mu'} = \dots = \sum_{\mu'} \hat{J}_{i_1 \dots i_{N_v}}^{\mu_1 \dots \mu'} = 0, \quad (8)$$

for all i, i_1, \dots, i_{N_v} and μ_1, \dots, μ_{N_v} .

Although a gauge transformation does not alter the Boltzmann distribution, other functions of model parameters, such as the n -th order couplings Fröbenius norm, $F^{(n)} = \left[\sum_{\mu_1, \dots, \mu_n} (J_{i_1 \dots i_n}^{\mu_1 \dots \mu_n})^2 \right]^{\frac{1}{2}}$, is gauge-dependent. In practice, the zero-sum gauge is widely used in inference applications because it minimizes the strength of high-order couplings by favoring the contribution of low-order couplings [8]. This is also important for the interpretability of models with all-order interactions because, in such situations, one would want to compute an effective low-order Hamiltonian that approximates as well as possible the complete effective Hamiltonian [15].

Effective Couplings of an RBM.— Expanding the marginal Hamiltonian (5) gives an effective generalized Potts model, as described in (6) (Appendix B). The general expression for n -th order effective coupling obtained in such expansion is

$$J_{i_1 \dots i_n}^{\mu_1 \dots \mu_n} = \sum_{K \subseteq [n]} (-1)^{n-|K|} \left[\sum_a \ln \left(1 + e^{c_a + \sum_{k \in K} W_{i_k a}^{\mu_k}} \right) \right], \quad (9)$$

where we introduced the set $[n] = \{1, 2, \dots, n\}$ and $|A|$ to denote the cardinal (i.e., the number of elements) of a given set A . The expression (9) generalizes to categorical variables those that were previously derived for the effective couplings of the binary case in the lattice-gas gauge [19, 20]. Since it is much more sensible to consider the zero-sum gauge for inference and interpretability applications, we transformed expressions (9) to the zero-sum gauge (Appendix C) to obtain

$$\begin{aligned} \hat{J}_{i_1 \dots i_n}^{\mu_1 \dots \mu_n} &= \sum_{K \subseteq [n]} (-1)^{n-|K|} \left[\frac{1}{q^{N_v}} \sum_{\mu'_1, \dots, \mu'_{N_v}} \sum_a \right. \\ &\quad \left. \ln \left(1 + e^{c_a + \sum_{k \in K} W_{i_k a}^{\mu_k} + \sum_{l \in [N_v] \setminus K} W_{i_l a}^{\mu'_l}} \right) \right]. \end{aligned} \quad (10)$$

The above mapping is easily generalizable to any probabilistic model defined on high-dimension categorical space. Formally, any probability mass function π defined over $\Omega \equiv \{1, 2, \dots, q\}^{N_v}$, such that $\pi(\mathbf{v}) > 0 \forall \mathbf{v} \in \Omega$, can be mapped into a multibody generalized Potts model (6), whose n -th order couplings are given by

$$J_{i_1 \dots i_n}^{\mu_1 \dots \mu_n} = \sum_{K \subseteq [n]} (-1)^{n-|K|} \mathbb{E}_{\mathbf{u} \sim G} [\ln \pi(\mathbf{u}) | u_{i_k} = \mu_k : k \in K], \quad (11)$$

where, $\mathbb{E}_{\mathbf{u} \sim G} [f(\mathbf{u}) | u_{i_k} = \mu_k : k \in K]$ is the expected value of a function $f : \Omega \rightarrow \mathbb{R}$ with $\mathbf{v} \in \Omega$ following an arbitrary probability measure G but keeping $v_{i_k} = \mu_k$, with $k \in K$. The arbitrariness in G choice reflects the gauge

invariance mentioned earlier. For instance, the lattice gas gauge condition (7) is obtained by considering that G is the degenerate distribution that assigns probability 1 to the configuration (q, q, \dots, q) and 0 to any other $\mathbf{v} \in \Omega$. Moreover, we have the zero-sum gauge if G is uniformly distributed over Ω . It is easy to check that we can recover expressions (9) and (10) by replacing $\pi(\mathbf{v}) \propto \exp \left[-\sum_a \ln \left(1 + e^{c_a + \sum_{i, \mu} W_{i a}^{\mu} \delta_{\mu}^{v_i}} \right) \right]$ in (11) considering G either as the degenerate or the uniform distribution, respectively. A general proof of the Potts equivalence and gauge fixing using (11) is provided in App. D.

In general, the computation of the effective couplings of any order in the zero-sum gauge requires computing the average of q^{N_v} elements, which is computationally prohibitive in most real-world applications. Previous approaches have extracted pairwise interactions of energy-based models by approximating this average with samples [15, 24], which is computationally too heavy to compute higher-order interactions. The ref. [22] introduces an approach that leverages the structure of the energy function of the RBM and the Central Limit Theorem (CLT) to approximate the terms inside brackets in (10) [22]. Using such an approach to compute the n -th order couplings, we first reduce the sum over all possible configurations, which has q^{N_v} elements, to a sum over q^n elements by considering the following identity

$$\begin{aligned} &\frac{1}{q^{N_v}} \sum_{\mu'_1, \dots, \mu'_{N_v}} \ln \left(1 + e^{c_a + \sum_{k=1}^{N_v} W_{i_k a}^{\mu'_k}} \right) \\ &= \frac{1}{q^n} \sum_{\mu'_1, \dots, \mu'_{N_v}} \mathbb{E}_{x \sim X} \left[\ln \left(1 + e^{c_a + \sum_{k=1}^n W_{i_k a}^{\mu'_k} + x} \right) \right], \end{aligned} \quad (12)$$

where, $X \equiv \sum_{k=n+1}^{N_v} W_{i_k a}^*$, such that $W_{i_k a}^*$ is a random variable uniformly distributed over $\{W_{i_k a}^{\mu} : \mu \in [q]\}$. Then, by using the central limit theorem and the zero-sum parameters of the RBM, we approximate the r.h.s of (12) through the following integral

$$\frac{1}{\sqrt{2\pi}\sigma} \int_{-\infty}^{\infty} dx e^{-\frac{x^2}{2\sigma^2}} \ln \left(1 + e^{c_a + \sum_{k=1}^n W_{i_k a}^{\mu_k} + x} \right)$$

with $\sigma = \left[q^{-1} \sum_{k=n+1}^{N_v} \sum_{\mu=1}^q W_{i_k a}^{\mu} \right]^{\frac{1}{2}}$. The above integral can be approximated using numerical methods, and, in our tests, using 20 steps has been enough to obtain reliable estimates. We further speed up the code by parallel computation of the q^n couplings among the n sites.

Inverse Numerical Experiments—We evaluate our approach through an inverse experiment using a spin-1 Blume-Capel model with 2-body and 3-body interactions. The ground-truth Hamiltonian is:

$$\mathcal{H}_D(\mathbf{s}) = -J^{(3)} \sum_{\langle ijk \rangle} s_i s_j s_k - J^{(2)} \sum_{\langle ij \rangle} s_i s_j, \quad (13)$$

where $s_i \in \{-1, 0, 1\}$. The dataset is generated by sampling from the Boltzmann distribution at inverse temperature $\beta = 0.2$. For the experiments, we simulated a 1D

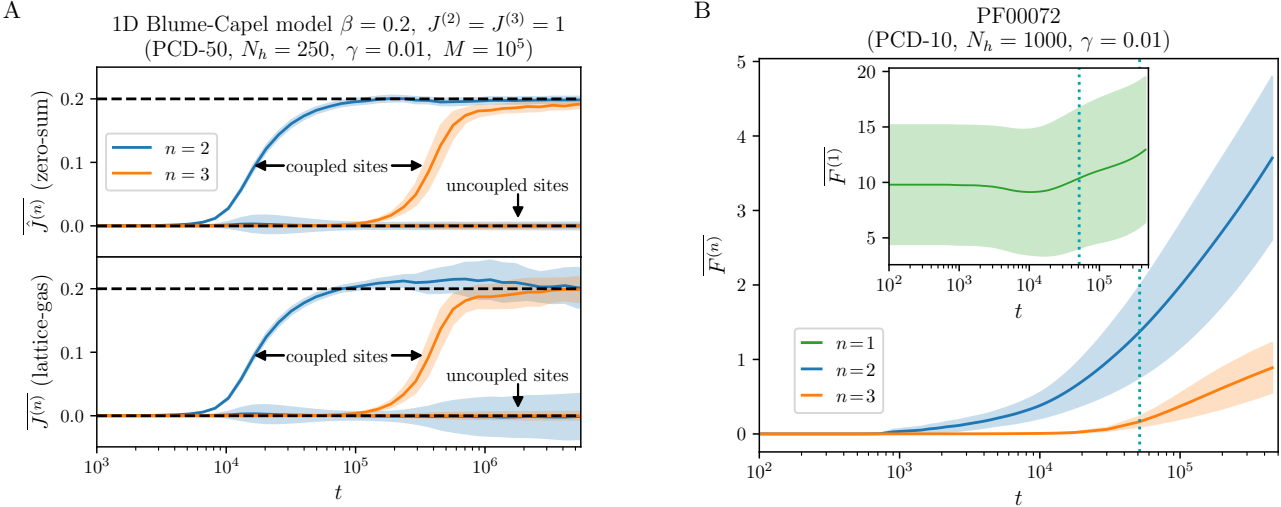


FIG. 1. **Learning dynamics of the effective model.** For an RBM trained with samples of a spin-1 Blume-Capel model with three body interactions defined in Eq. (13) with $J^{(2)} = J^{(3)} = 1$ at inverse temperature $\beta = 0.2$, (A) shows the evolution of the averaged effective couplings extracted from the RBM along the training time t in both the zero-sum (*top*) and lattice gas (*bottom*) gauges. For an RBM trained with the MSA of the PF00072 protein family, (B) displays the Fröbenius norm of the inferred effective model parameters as a function of the training time. We point out the update when we obtain a maximum in the contact prediction performance with the vertical dashed line. In both figures, the solid lines indicate mean values, and the width of the shading areas indicates the standard deviation.

chain of $N = 51$ spins with periodic boundary conditions ($s_{N+1} \equiv s_1$), fixing pairwise nearest-neighbor interactions with $J^{(2)} = 1$ and adding sparse 3-spin interactions at distant sites with $J^{(3)} = 1$. Specifically, triads involve sites i, j, k satisfying $i \equiv j \equiv k \pmod{17}$. This 3-state Potts model is particularly appealing as it simultaneously satisfies the zero-sum (8) and lattice gas (7) gauges.

We train a binary-Potts RBM with 250 hidden nodes and extract two- and three-body couplings using (9) (lattice gas gauge) and (10) (zero-sum gauge), comparing them to true values for coupling and non-coupling links. Fig. 1-A shows that RBMs sequentially learn interactions from lower to higher orders, independent of the gauge. This aligns with findings in binary RBMs [22] and transformers on language data [25]. The zero-sum gauge yields more precise values, confirming its superiority for inference and interpretability.

rbmDCA.— One of the most celebrated applications of the inverse Potts problem is predicting contact sites in protein tertiary structures from MSA data [8]. To explore this, we trained an RBM on the MSA of the response regulator domain family (Pfam entry: PF00072) [26] and used our zero-sum mapping to compute contact map predictions during training (Fig. 1-B). These maps were compared against a known 3D structure of the domain and evaluated against established DCA methods, including plmDCA [27, 28], based on pseudo-likelihood maximization and adabmDCA [29, 30], based on Boltzmann machine learning (Fig. 2).

To assess RBM learning convergence on this dataset, we calculated the log-likelihood (LL) during training us-

ing a split dataset (60% training, 40% test). LL was approximated using the Trajectory Annealing Importance Sampling method [31] (Fig. 2-C). In Figure 2-D, we observe that the performance of the RBM training increments with the training time t until it reaches a maximum, where its inference is comparable with other state-of-the-art methods. In particular, we note a similar performance with the adabmDCA, while plmDCA overperforms both. Beyond this point, the prediction performance of the RBM decreases with t due to overfitting. Fig. 2-C shows that near before the maximum, the log-likelihood w.r.t. the validation set lags behind the increments of the log-likelihood w.r.t. the training. Another indication for overfitting is in Fig. 1-B, where we see that coupling parameters at all orders do not stabilize but keep growing with t even after the best inference is reached. We also note this worsening of the performance also coincides with the learning three-wise of effective couplings (see Figure 1 B) and a slowing down in the sampling dynamics of the RBM (i.e., a considerable increment in the mixing time of the model), which accounts for the occurrence non-equilibrium effects [32, 33]. All of the above seems to indicate that, after getting a good representation of the data, the model would fit very low frequencies and co-occurrences with infinitely large and negative effective fields and couplings. A solution for this could be implementing a pseudo-count strategy for the RBM log-likelihood function, which will be left for future work.

Conclusions.— This paper presented a general framework for interpreting generative models defined on high-

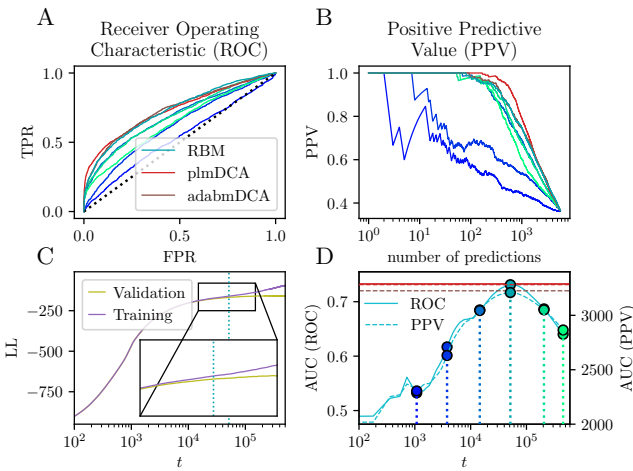


FIG. 2. Contact Prediction from the MSA. Considering the PF00072 protein family, (A) and (B) show the receiver operating characteristic curve (ROC curve) and the positive predictive value against the number of predictions (PPV curve) at the different stages of the training. (C) display the log-likelihood (LL) concerning the training set and a validation set during the training. In (D), we plotted the area under the ROC and PPV curves versus the training time t . Colored dots and lines in (D) correspond to the different training stages shown in (A) and (B). The models shown here were trained using a PCD-10 scheme, 1000 hidden nodes, and a 0.01 learning rate.

dimensional categorical data in terms of a Potts model with many-body interactions. Using this framework, we developed and implemented a protocol that leverages the energy structure of the RBM to extract multi-body couplings from observations. We conducted a controlled experiment in which we successfully extracted the multi-body couplings from synthetic data samples from a modified version of the Blume-Capel model with 2-body and 3-body interactions. In this first experiment, we verified that the coupling learning is sequential, i.e., $(n+1)$ -body interaction is learned after n -body is learned, a feature recently found in deep transformers [25]. Then, we tested the robustness of our approach with the MSA of a protein family. In this case, we verified that the effective pairwise models extracted from RBM learning could be used to reconstruct the contact map of the tertiary protein structure, achieving performance comparable with state-of-the-art methods. Despite these promising results, we also found overfitting problems due to the learning of large negative couplings due to the low frequency of some states. The treatment of these convergence problems will be left for future work.

[1] A. De Martino and D. De Martino, An introduction to the maximum entropy approach and its application to inference problems in biology, *Heliyon* **4** (2018).

[2] E. Schneidman, M. J. Berry, R. Segev, and W. Bialek, Weak pairwise correlations imply strongly correlated network states in a neural population, *Nature* **440**, 1007 (2006).

[3] Y. Roudi, E. Aurell, and J. A. Hertz, Statistical physics of pairwise probability models, *Frontiers in computational neuroscience* **3**, 652 (2009).

[4] L. Meshulam, J. L. Gauthier, C. D. Brody, D. W. Tank, and W. Bialek, Collective behavior of place and non-place neurons in the hippocampal network, *Neuron* **96**, 1178 (2017).

[5] O. Maoz, G. Tkačik, M. S. Esteki, R. Kiani, and E. Schneidman, Learning probabilistic neural representations with randomly connected circuits, *Proceedings of the National Academy of Sciences* **117**, 25066 (2020).

[6] T. R. Lezon, J. R. Banavar, M. Cieplak, A. Maritan, and N. V. Fedoroff, Using the principle of entropy maximization to infer genetic interaction networks from gene expression patterns, *Proceedings of the National Academy of Sciences* **103**, 19033 (2006).

[7] G. Tkačik, C. G. Callan Jr, and W. Bialek, Information flow and optimization in transcriptional regulation, *Proceedings of the National Academy of Sciences* **105**, 12265 (2008).

[8] S. Cocco, C. Feinauer, M. Figliuzzi, R. Monasson, and M. Weigt, Inverse statistical physics of protein sequences: a key issues review, *Reports on Progress in Physics* **81**, 032601 (2018).

[9] F. Morcos, A. Pagnani, B. Lunt, A. Bertolino, D. S. Marks, C. Sander, R. Zecchina, J. N. Onuchic, T. Hwa, and M. Weigt, Direct-coupling analysis of residue coevolution captures native contacts across many protein families, *Proceedings of the National Academy of Sciences* **108**, E1293 (2011).

[10] M. Weigt, R. A. White, H. Szurmant, J. A. Hoch, and T. Hwa, Identification of direct residue contacts in protein–protein interaction by message passing, *Proceedings of the National Academy of Sciences* **106**, 67 (2009).

[11] J. Harte, *Maximum entropy and ecology: a theory of abundance, distribution and species richness* (OUP Oxford, 2011).

[12] F. Battiston, E. Amico, A. Barrat, G. Bianconi, G. Ferri, F. de Arruda, B. Franceschiello, I. Iacopini, S. Kéfi, V. Latora, Y. Moreno, et al., The physics of higher-order interactions in complex systems, *Nature Physics* **17**, 1093 (2021).

[13] J. Jumper, R. Evans, A. Pritzel, T. Green, M. Figurnov, O. Ronneberger, K. Tunyasuvunakool, R. Bates, A. Žídek, A. Potapenko, et al., Highly accurate protein structure prediction with alphafold, *nature* **596**, 583 (2021).

[14] J. Abramson, J. Adler, J. Dunger, R. Evans, T. Green, A. Pritzel, O. Ronneberger, L. Willmore, A. J. Ballard, J. Bambrick, et al., Accurate structure prediction of biomolecular interactions with alphafold 3, *Nature* **1**, 1 (2024).

[15] C. Feinauer, B. Meynard-Piganeau, and C. Lucibello, Interpretable pairwise distillations for generative protein sequence models, *PLOS Computational Biology* **18**, e1010219 (2022).

[16] F. Caredda and A. Pagnani, Direct coupling analysis and the attention mechanism, *bioRxiv* , 2024 (2024).

[17] P. Smolensky, In parallel distributed processing: Volume 1 by d. rumelhart and j. mclelland (MIT Press, 1986) Chap. 6: Information Processing in Dynamical Systems: Foundations of Harmony Theory.

[18] N. Le Roux and Y. Bengio, Representational power of restricted boltzmann machines and deep belief networks, *Neural computation* **20**, 1631 (2008).

[19] G. Cossu, L. Del Debbio, T. Giani, A. Khamseh, and M. Wilson, Machine learning determination of dynamical parameters: The ising model case, *Physical Review B* **100**, 064304 (2019).

[20] N. Bulso and Y. Roudi, Restricted boltzmann machines as models of interacting variables, *Neural Computation* **33**, 2646 (2021).

[21] S. Feng, D. Kong, and N. Trivedi, A statistical approach to topological entanglement: Boltzmann machine representation of high-order irreducible correlation, *arXiv preprint arXiv:2302.03212* (2023).

[22] A. Decelle, C. Furtlehner, A. d. J. Navas Gómez, and B. Seoane, Inferring effective couplings with restricted boltzmann machines, *SciPost Physics* **16**, 095 (2024).

[23] S. Cocco, A. De Martino, A. Pagnani, M. Weigt, and F. Ritort, Statistical physics of biological molecules, *Spin Glass Theory and Far Beyond: Replica Symmetry Breaking After 40 Years* , 523 (2023).

[24] J. Tubiana, S. Cocco, and R. Monasson, Learning protein constitutive motifs from sequence data, *Elife* **8**, e39397 (2019).

[25] R. Rende, F. Gerace, A. Laio, and S. Goldt, A distributional simplicity bias in the learning dynamics of transformers, *arXiv preprint arXiv:2410.19637* (2024).

[26] J. Trinquier, G. Uguzzoni, A. Pagnani, F. Zamponi, and M. Weigt, Efficient generative modeling of protein sequences using simple autoregressive models, *Nature communications* **12**, 5800 (2021).

[27] M. Ekeberg, C. Lövkist, Y. Lan, M. Weigt, and E. Aurell, Improved contact prediction in proteins: using pseudolikelihoods to infer potts models, *Physical Review E—Statistical, Nonlinear, and Soft Matter Physics* **87**, 012707 (2013).

[28] M. Ekeberg, T. Hartonen, and E. Aurell, Fast pseudolikelihood maximization for direct-coupling analysis of protein structure from many homologous amino-acid sequences, *Journal of Computational Physics* **276**, 341 (2014).

[29] A. P. Muntoni, A. Pagnani, M. Weigt, and F. Zamponi, adabmdca: adaptive boltzmann machine learning for biological sequences, *BMC bioinformatics* **22**, 1 (2021).

[30] L. Rosset, R. Netti, A. P. Muntoni, M. Weigt, and F. Zamponi, adabmdca 2.0: A flexible but easy-to-use package for direct coupling analysis, (2024).

[31] N. Béreux, A. Decelle, C. Furtlehner, L. Rosset, and B. Seoane, Fast, accurate training and sampling of restricted boltzmann machines, *arXiv preprint arXiv:2405.15376* (2024).

[32] A. Decelle, C. Furtlehner, and B. Seoane, Equilibrium and non-equilibrium regimes in the learning of restricted boltzmann machines, *Advances in Neural Information Processing Systems* **34**, 5345 (2021).

[33] E. Agoritsas, G. Catania, A. Decelle, and B. Seoane, Explaining the effects of non-convergent sampling in the training of energy-based models, in *ICML 2023-40th International Conference on Machine Learning* (2023).

[34] T. Tielemans, Training restricted boltzmann machines using approximations to the likelihood gradient, in *Proceedings of the 25th international conference on Machine learning* (2008) pp. 1064–1071.

[35] C. Feinauer and E. Borgonovo, Mean dimension of generative models for protein sequences, *bioRxiv* , 2022 (2022).

[36] J. Fernandez-de Cossio-Diaz, Generative modeling of rna sequence families with restricted boltzmann machines, in *RNA Design: Methods and Protocols* (Springer, 2024) pp. 163–175.

[37] C. W. Lynn, Q. Yu, R. Pang, S. E. Palmer, and W. Bialek, Exact minimax entropy models of large-scale neuronal activity, *arXiv preprint arXiv:2402.00007* (2023).

[38] D. H. Ackley, G. E. Hinton, and T. J. Sejnowski, A learning algorithm for Boltzmann machines, *Cognitive science* **9**, 147 (1985).

[39] M. Figliuzzi, P. Barrat-Charlaix, and M. Weigt, How pairwise coevolutionary models capture the collective residue variability in proteins?, *Molecular biology and evolution* **35**, 1018 (2018).

[40] S. Zamuner and P. D. L. Rios, Interpretable neural networks based classifiers for categorical inputs, *arXiv preprint arXiv:2102.03202* (2021).

[41] M. Blume, Theory of the first-order magnetic phase change in u o 2, *Physical Review* **141**, 517 (1966).

[42] H. Capel, On the possibility of first-order phase transitions in ising systems of triplet ions with zero-field splitting, *Physica* **32**, 966 (1966).

Appendix A: Training of the RBM

The RBM is trained by maximizing the log-likelihood function \mathcal{L} of the observation of a given dataset $\mathcal{D} = \{\mathbf{v}^{(1)}, \dots, \mathbf{v}^{(M)}\}$ with probabilistic model parameters Θ . This means that our goal is to maximize

$$\mathcal{L}(\Theta|\mathcal{D}) = \frac{1}{M} \sum_{m=1}^M \log p_{\Theta}(\mathbf{v}^{(m)}) = \frac{1}{M} \sum_{m=1}^M \log \sum_{\mathbf{h}} e^{-\mathcal{H}_{\Theta}(\mathbf{v}^{(m)}, \mathbf{h})} - \log Z_{\Theta}, \quad (\text{A1})$$

which is done using (stochastic) gradient descent. For our RBM, this gradient reads as follows

$$\begin{aligned} \frac{\partial \mathcal{L}}{\partial b_i^{\mu}} &= \langle \delta_{\mu}^{v_i} \rangle_{\mathcal{D}} - \langle \delta_{\mu}^{v_i} \rangle_{\mathcal{H}}, \quad \frac{\partial \mathcal{L}}{\partial c_a} = \langle h_a \rangle_{\mathcal{D}} - \langle h_a \rangle_{\mathcal{H}}, \\ \text{and} \quad \frac{\partial \mathcal{L}}{\partial W_{ia}^{\mu}} &= \langle h_a \delta_{\mu}^{v_i} \rangle_{\mathcal{D}} - \langle h_a \delta_{\mu}^{v_i} \rangle_{\mathcal{H}}, \end{aligned} \quad (\text{A2})$$

where $\langle \dots \rangle_{\mathcal{D}}$ and $\langle \dots \rangle_{\mathcal{H}}$ represents respectively the average computed over the dataset and the Boltzmann distribution with the Hamiltonian defined as in (2). We also used h_a to shorten $p(h_a = 1|\mathbf{v})$, the conditional probability of the hidden variable being $h_a = 1$ given a fixed configuration of the visible variables \mathbf{v} . Since computing the partition function is typically intractable, the second average is approximated using the Block-Gibbs Sampling Markov Chain Monte Carlo (MCMC) method. This method uses the bipartite structure of the lattice to iteratively sample the visible and hidden variables, conditional on the other layer, which allows high parallelization.

In this work, we consistently used the persistent contrastive divergence (PCD- k) method [34]. The initial states of the parallel Markov chains used for gradient computation are taken from the final states obtained in the previous parameter update. The number of steps in each update is fixed at k . Numerical investigations have shown that this approach can yield quasi-equilibrium models [32]. We also verified that the learned models operated in the equilibrium regime [32, 33], with no memory of the training scheme.

Appendix B: Deriving the Effective lattice gas Model

In Ref. [19] a Bernoulli-Bernoulli RBM (i.e., $v_i, h_a \in \{0, 1\}$) was mapped into a multi-body Ising-like model of binary variables. The following section uses such an analogous approach to derive a mapping considering an arbitrary q . Marginalizing the Boltzmann distribution (1) gives

$$p(\mathbf{v}) = \frac{1}{Z} \sum_{\mathbf{h}} e^{-\mathcal{H}(\mathbf{v}, \mathbf{h})} = \frac{1}{Z} e^{-\mathcal{H}(\mathbf{v})}. \quad (\text{B1})$$

Then, we solve $\mathcal{H}(\mathbf{v})$ from the above expression and replace the RBM Hamiltonian defined in (2) to obtain

$$\mathcal{H}(\mathbf{v}) = - \sum_{i,\mu} b_i^{\mu} \delta_{\mu}^{v_i} - \sum_a \ln \sum_{h_a} e^{c_a h_a + h_a \sum_{i,\mu} W_{ia}^{\mu} \delta_{\mu}^{v_i}}. \quad (\text{B2})$$

By defining

$$q(h_a) \equiv e^{c_a h_a} \text{ and } t \equiv \sum_{i,\mu} W_{ia}^{\mu} \delta_{\mu}^{v_i}, \quad (\text{B3})$$

we introduce the following cumulant-generating function

$$K_a(t) \equiv \ln \sum_{h_a} q(h_a) e^{h_a t} = \sum_{k=0}^{\infty} \frac{\kappa_a^{(k)} t^k}{k!} \quad (\text{B4a})$$

$$= \ln (1 + e^{c_a + t}), \quad (\text{B4b})$$

where the k -th cumulant is

$$\kappa_a^{(k)} = \left. \frac{\partial^k K_a(t)}{\partial t^k} \right|_{t=0}. \quad (\text{B5})$$

Replacing (B4a), in (B2) gives

$$\mathcal{H}(\mathbf{v}) = - \sum_{i,\mu} b_i^\mu \delta_\mu^{v_i} - \sum_{a,k} \frac{\kappa_a^{(k)} t^k}{k!}.$$

Considering the definition (B3), we rewrite the above expression as

$$\mathcal{H}(\mathbf{v}) = - \sum_a \kappa_a^{(0)} - \sum_{i,a} \left(b_i^\mu + \sum_a \kappa_i^{(1)} W_{ia}^\mu \right) \delta_\mu^{v_i} - \sum_{k>1} \frac{1}{k!} \sum_{i_1, \dots, i_k} \sum_{\mu_1, \dots, \mu_k} \left(\sum_a \kappa_a^{(k)} W_{i_1 a}^{\mu_1} \cdots W_{i_k a}^{\mu_k} \right) \delta_{\mu_1}^{v_{i_1}} \cdots \delta_{\mu_k}^{v_{i_k}}. \quad (\text{B6})$$

Here, we note that high-order terms in k also contribute to the n -body coupling constants, where n is the number of distinct sites. Since

$$\delta_{\mu_1}^{v_i} \delta_{\mu_2}^{v_i} \cdots \delta_{\mu_k}^{v_i} = \begin{cases} \delta_\mu^{v_i} & \text{if } \mu = \mu_1 = \mu_2 = \cdots = \mu_k \\ 0 & \text{otherwise,} \end{cases}$$

high-order terms cancel out if they include factors of visible variables with different colors on the same site. Then, for each k in (B6), the sum over the visible sites i_1, \dots, i_k can be grouped by the number n of distinct sites being considered. Thus, the term of (B6) that includes solely sites i_1 and i_2 , considering the contributions of all orders in k , is given by

$$\begin{aligned} & \sum_{k>1} \frac{1}{k!} \sum_{l=1}^{k-1} \sum_{1 \leq i_1 < i_2 \leq N_v} \sum_{\mu_1, \mu_2} \left(\sum_a \kappa_a^{(k)} \binom{k}{l} (W_{i_1 a}^{\mu_1})^l (W_{i_2 a}^{\mu_2})^{k-l} \right) \delta_{\mu_1}^{v_{i_1}} \delta_{\mu_2}^{v_{i_2}} \\ &= \sum_{k>1} \frac{1}{k!} \sum_{1 \leq i_1 < i_2 \leq N_v} \sum_{\mu_1, \mu_2} \left(\sum_a \kappa_a^{(k)} \left[(W_{i_1 a}^{\mu_1} + W_{i_2 a}^{\mu_2})^k - (W_{i_1 a}^{\mu_1})^k - (W_{i_2 a}^{\mu_2})^k \right] \right) \delta_{\mu_1}^{v_{i_1}} \delta_{\mu_2}^{v_{i_2}}. \end{aligned}$$

The direct comparison of the above with (6) implies that

$$J_{i_1 i_2}^{\mu_1 \mu_2} = \sum_{k>1} \frac{1}{k!} \sum_a \kappa_a^{(k)} \left[(W_{i_1 a}^{\mu_1} + W_{i_2 a}^{\mu_2})^k - (W_{i_1 a}^{\mu_1})^k - (W_{i_2 a}^{\mu_2})^k \right]. \quad (\text{B7})$$

Replacing (B5) in (B7) gives

$$\begin{aligned} J_{i_1 i_2}^{\mu_1 \mu_2} &= \sum_{k>1} \frac{1}{k!} \sum_a \left[(W_{i_1 a}^{\mu_1} + W_{i_2 a}^{\mu_2})^k - (W_{i_1 a}^{\mu_1})^k - (W_{i_2 a}^{\mu_2})^k \right] \frac{\partial^k K_a(t)}{\partial t^k} \Big|_{t=0} \\ &= \sum_a \sum_k \frac{1}{k!} \left[(W_{i_1 a}^{\mu_1} + W_{i_2 a}^{\mu_2})^k - (W_{i_1 a}^{\mu_1})^k - (W_{i_2 a}^{\mu_2})^k \right] \frac{\partial^k K_a(t)}{\partial t^k} \Big|_{t=0} + \sum_a K_a(0) \\ &= \sum_i \left[e^{(W_{i_1 a}^{\mu_1} + W_{i_2 a}^{\mu_2}) \partial_t} - e^{W_{i_1 a}^{\mu_1} \partial_t} - e^{W_{i_2 a}^{\mu_2} \partial_t} + 1 \right] K_i(t) \Big|_{t=0}. \end{aligned}$$

In the above expression, we identify the shift (or translation) operator

$$e^{a \partial_x} f(x) = f(a + x), \quad (\text{B8})$$

which gives us

$$J_{i_1 i_2}^{\mu_1 \mu_2} = \sum_a \left[K_a (W_{i_1 a}^{\mu_1} + W_{i_2 a}^{\mu_2}) - K_a (W_{i_1 a}^{\mu_1}) - K_a (W_{i_2 a}^{\mu_2}) + K_a(0) \right]. \quad (\text{B9})$$

Using definition (B4b) in (B9) leads automatically to

$$J_{i_1 i_2}^{\mu_1 \mu_2} = \sum_a \ln \frac{\left(1 + e^{c_a + W_{i_1 a}^{\mu_1} + W_{i_2 a}^{\mu_2}} \right) (1 + e^{c_a})}{\left(1 + e^{c_a + W_{i_1 a}^{\mu_1}} \right) \left(1 + e^{c_a + W_{i_2 a}^{\mu_2}} \right)}. \quad (\text{B10})$$

Similarly, the field contributions in (B6) can be written as

$$-\sum_{i,\mu} \left(b_i^\mu + \sum_a \kappa_a^{(1)} W_{i1a}^\mu \right) \delta_\mu^{v_i} - \sum_{k>1} \frac{1}{k!} \sum_{i,\mu} \left(\sum_a \kappa_a^{(k)} (W_{i1a}^\mu)^k \right) \delta_\mu^{v_i}. \quad (\text{B11})$$

Developing the left-side term in the above:

$$\begin{aligned} \sum_{k>1} \frac{1}{k!} \sum_a \kappa_a^{(k)} (W_{i1a}^\mu)^k &= \sum_{k \geq 0} \frac{1}{k!} \sum_a (W_{ia}^\mu)^k \frac{\partial^k K_a(t)}{\partial t^k} \Big|_{t=0} - \sum_a K_a(0) - \sum_a \kappa_a^{(1)} W_{ia}^\mu \\ &= \sum_a e^{W_{ia}^\mu \partial_t} K_a(t) \Big|_{t=0} - \sum_a K_a(0) - \sum_a \kappa_a^{(1)} W_{ia}^\mu \\ &= \sum_a \left[K_i(W_{ia}^\mu) - K_a(0) - \kappa_i^{(1)} W_{ia}^\mu \right] \\ &= \sum_a \left[\ln \left(\frac{1 + e^{c_a + W_{ia}^\mu}}{1 + e^{c_a}} \right) - \kappa_i^{(1)} W_{ia}^\mu \right]. \end{aligned} \quad (\text{B12})$$

Finally, substituting (B12) in (B11) and comparing with (6) we obtain that the effective fields are given by

$$H_i^\mu = b_i^\mu + \sum_a \ln \left(\frac{1 + e^{c_a + W_{ia}^\mu}}{1 + e^{c_a}} \right) \equiv b_i^\mu + J_i^\mu, \quad (\text{B13})$$

where we denoted by J_i^μ the contribution to the effective fields due to the interaction with the hidden variables. An analogous procedure can be applied considering the contributions from all k -orders to any n -th order interaction in (B6) to derive the corresponding coupling constant, whose general expression is given by (9).

Finally, to verify that the couplings written in this formulation satisfy the lattice gas condition (7), we set the RBM in its corresponding lattice gas gauge (i.e., $b_j^q = W_{ij}^q = 0$ for all i, j) then it is easy to see that

$$\begin{aligned} H_i^q &= b_i^q + \sum_a \ln \left(\frac{1 + e^{c_a + W_{ia}^q}}{1 + e^{c_a}} \right) = 0, \text{ and} \\ J_{i_1 i_2}^{\mu_1 q} &= \sum_a \ln \frac{\left(1 + e^{c_a + W_{i_1 a}^{\mu_1} + W_{i_2 a}^q} \right) (1 + e^{c_a})}{\left(1 + e^{c_a + W_{i_1 a}^{\mu_1}} \right) \left(1 + e^{c_a + W_{i_2 a}^q} \right)} = 0. \end{aligned}$$

Thus, in general, we have

$$J_{i_1 \dots i_n}^{\mu_1 \dots q} = \sum_{K \subseteq [n-1]} \sum_a \left[(-1)^{n-|K|} \ln \left(1 + e^{c_a + \sum_{k \in K} W_{i_k a}^{\mu_k}} \right) - (-1)^{n-|K|} \ln \left(1 + e^{c_a + \sum_{n \in K} W_{i_n a}^{\mu_k} + W_{i_n a}^q} \right) \right] = 0.$$

Appendix C: Deriving the Effective Zero-Sum Model

Since addressing gauge transformation of the model (6) for a general RBM directly can be challenging, let us start with a more approachable system: a hidden node connected just to three visible variables (see Fig. 3). In this case, the effective Potts Hamiltonian includes up to 3-body interactions:

$$\mathcal{H}(\mathbf{v}) = - \sum_{i,\mu} H_i^\mu \delta_\mu^{v_i} - \sum_{i_1 < i_2} \sum_{\mu_1, \mu_2} J_{i_1 i_2}^{\mu_1 \mu_2} \delta_{\mu_1}^{v_{i_1}} \delta_{\mu_2}^{v_{i_2}} - \sum_{i_1 < i_2 < i_3} \sum_{\mu_1, \mu_2, \mu_3} J_{i_1 i_2 i_3}^{\mu_1 \mu_2 \mu_3} \delta_{\mu_1}^{v_{i_1}} \delta_{\mu_2}^{v_{i_2}} \delta_{\mu_3}^{v_{i_3}}. \quad (\text{C1})$$

Without loss of generality, we assume that the above Hamiltonian is written in the lattice gas gauge as derived in the Appendix B. We obtain effective pairwise couplings and fields in the zero-sum gauge by applying the following gauge

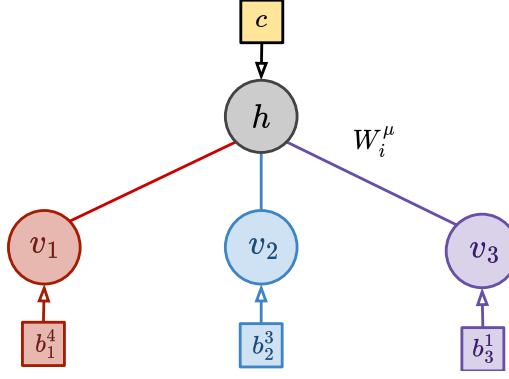


FIG. 3. Diagram of the 3-visible hidden nodes RBM we use to derive the exact mapping in the zero-sum Gauge.

transformations:

$$\begin{aligned} \hat{J}_{i_1 i_2}^{\mu_1 \mu_2} &\equiv J_{i_1 i_2}^{\mu_1 \mu_2} - \frac{1}{q} \left(\sum_{\mu'_1} J_{i_1 i_2}^{\mu'_1 \mu_2} + \sum_{\mu'_2} J_{i_1 i_2}^{\mu_1 \mu'_2} \right) + \frac{1}{q^2} \sum_{\mu'_1, \mu'_2} J_{i_1 i_2}^{\mu'_1 \mu'_2} \\ &+ \frac{1}{q} \sum_{\mu'_3} J_{i_1 i_2 i_3}^{\mu_1 \mu_2 \mu'_3} - \frac{1}{q^2} \left(\sum_{\mu'_1, \mu'_3} J_{i_1 i_2 i_3}^{\mu'_1 \mu_2 \mu'_3} + \sum_{\mu'_2, \mu'_3} J_{i_1 i_2 i_3}^{\mu_1 \mu'_2 \mu'_3} \right) + \frac{1}{q^3} \sum_{\mu'_1, \mu'_2, \mu'_3} J_{i_1 i_2 i_3}^{\mu'_1 \mu'_2 \mu'_3} \end{aligned} \quad (C2)$$

$$\begin{aligned} \hat{H}_{i_1}^{\mu_1} &\equiv H_{i_1}^{\mu_1} - \frac{1}{q} \sum_{\mu'_1} H_{i_1}^{\mu'_1} + \sum_{i_2} \left(\frac{1}{q} \sum_{\mu'_2} J_{i_1 i_2}^{\mu_1 \mu'_2} - \frac{1}{q^2} \sum_{\mu'_1, \mu'_2} J_{i_1 i_2}^{\mu'_1 \mu'_2} \right) \\ &+ \frac{1}{q^2} \sum_{\mu'_2, \mu'_3} J_{i_1 i_2 i_3}^{\mu_1 \mu'_2 \mu'_3} - \frac{1}{q^3} \sum_{\mu'_1, \mu'_2, \mu'_3} J_{i_1 i_2 i_3}^{\mu'_1 \mu'_2 \mu'_3}, \end{aligned} \quad (C3)$$

where, we always kept $i_1 \neq i_2, i_3$ and $i_2 \neq i_3$. Using the shift operation, introduced in (B8), we find the following recurrence relation in the general expression for couplings in the lattice gas gauge:

$$J_{i_1 \dots i_n}^{\mu_1 \dots \mu_n} = \left(e^{W_{i_n}^{\mu_n} \partial_c} - 1 \right) \sum_{K \subseteq [N-1]} (-1)^{n-1-|K|} \ln \left(1 + e^{c + \sum_{k \in K} W_{i_k}^{\mu_k}} \right) = \left(e^{W_{i_n}^{\mu_n} \partial_c} - 1 \right) J_{i_1 \dots i_{n-1}}^{\mu_1 \dots \mu_{n-1}}. \quad (C4)$$

Using (C4) to operate in (C2) gives

$$\begin{aligned} \hat{J}_{i_1 i_2}^{\mu_1 \mu_2} &= J_{i_1 i_2}^{\mu_1 \mu_2} - \frac{1}{q} \left(\sum_{\mu'_1} J_{i_1 i_2}^{\mu'_1 \mu_2} + \sum_{\mu'_2} J_{i_1 i_2}^{\mu_1 \mu'_2} \right) + \frac{1}{q^2} \sum_{\mu'_1, \mu'_2} J_{i_1 i_2}^{\mu'_1 \mu'_2} \\ &+ \frac{1}{q} \sum_{\mu'_3} \left(e^{W_{i_3}^{\mu'_3} \partial_c} - 1 \right) \left(J_{i_1 i_2}^{\mu_1 \mu_2} - \frac{1}{q} \left(\sum_{\mu'_1} J_{i_1 i_2}^{\mu'_1 \mu_2} + \sum_{\mu'_2} J_{i_1 i_2}^{\mu_1 \mu'_2} \right) + \frac{1}{q^2} \sum_{\mu'_1, \mu'_2} J_{i_1 i_2}^{\mu'_1 \mu'_2} \right) \\ &= \frac{1}{q} \sum_{\mu'_3} e^{W_{i_3}^{\mu'_3} \partial_c} \left(J_{i_1 i_2}^{\mu_1 \mu_2} - \frac{1}{q} \left(\sum_{\mu'_1} J_{i_1 i_2}^{\mu'_1 \mu_2} + \sum_{\mu'_2} J_{i_1 i_2}^{\mu_1 \mu'_2} \right) + \frac{1}{q^2} \sum_{\mu'_1, \mu'_2} J_{i_1 i_2}^{\mu'_1 \mu'_2} \right) \\ &= \frac{1}{q^3} \sum_{\mu'_1, \mu'_2, \mu'_3} e^{W_{i_3}^{\mu'_3} \partial_c} \left(J_{i_1 i_2}^{\mu_1 \mu_2} - J_{i_1 i_2}^{\mu'_1 \mu_2} - J_{i_1 i_2}^{\mu_1 \mu'_2} + J_{i_1 i_2}^{\mu'_1 \mu'_2} \right). \end{aligned} \quad (C5)$$

Then, we obtain the expression for the pairwise couplings in the zero-sum gauge by replacing (B10) in the above

$$\hat{J}_{i_1 i_2}^{\mu_1 \mu_2} = \frac{1}{q^3} \sum_{\mu'_1, \mu'_2, \mu'_3} \ln \frac{\left(1 + e^{c + W_{i_1}^{\mu_1} + W_{i_2}^{\mu_2} + W_{i_3}^{\mu'_3}} \right) \left(1 + e^{c + W_{i_1}^{\mu'_1} + W_{i_2}^{\mu'_2} + W_{i_3}^{\mu'_3}} \right)}{\left(1 + e^{c + W_{i_1}^{\mu_1} + W_{i_2}^{\mu'_2} + W_{i_3}^{\mu'_3}} \right) \left(1 + e^{c + W_{i_1}^{\mu'_1} + W_{i_2}^{\mu_2} + W_{i_3}^{\mu'_3}} \right)}. \quad (C6)$$

Similarly, for the fields, we can write

$$\begin{aligned}
\hat{H}_{i_1}^{\mu_1} &= b_{i_1}^{\mu_1} - \frac{1}{q} \sum_{\mu'_1} b_{i_1}^{\mu'_1} + J_{i_1}^{\mu_1} - \frac{1}{q} \sum_{\mu'_1} J_{i_1}^{\mu'_1} \\
&\quad - \frac{1}{q} \sum_{\mu'_3} \left(e^{W_{i_3}^{\mu'_3} \partial_c} - 1 \right) \left(J_{i_1}^{\mu_1} - \frac{1}{q} \sum_{\mu'_1} J_{i_1}^{\mu'_1} \right) - \frac{1}{q} \sum_{\mu'_2} \left(e^{W_{i_2}^{\mu'_2} \partial_c} - 1 \right) \left(J_{i_1}^{\mu_1} - \frac{1}{q} \sum_{\mu'_1} J_{i_1}^{\mu'_1} \right) \\
&\quad + \frac{1}{q^2} \sum_{\mu'_2, \mu'_3} \left(e^{W_{i_2}^{\mu'_2} \partial_c} - 1 \right) \left(e^{W_{i_3}^{\mu'_3} \partial_c} - 1 \right) \left(J_{i_1}^{\mu_1} - \frac{1}{q} \sum_{\mu'_1} J_{i_1}^{\mu'_1} \right) \\
&= b_{i_1}^{\mu_1} - \frac{1}{q} \sum_{\mu'_1} b_{i_1}^{\mu'_1} + \frac{1}{q^3} \sum_{\mu_1, \mu'_2, \mu'_1} e^{\left(W_{i_2}^{\mu'_2} + W_{i_3}^{\mu'_3} \right) \partial_c} \left(J_{i_1}^{\mu_1} - J_{i_1}^{\mu'_1} \right). \tag{C7}
\end{aligned}$$

Replacing the lattice gas coupling definition given in (B13) in the above gives

$$\hat{H}_{i_1}^{\mu_1} = \hat{b}_{i_1}^{\mu_1} + \frac{1}{q^3} \sum_{\mu'_1, \mu'_2, \mu'_3} \ln \left(\frac{1 + e^{c_a + W_{i_1}^{\mu_1} + W_{i_2}^{\mu'_2} + W_{i_3}^{\mu'_3}}}{1 + e^{c_a + W_{i_1}^{\mu'_1} + W_{i_2}^{\mu'_2} + W_{i_3}^{\mu'_3}}} \right), \tag{C8}$$

where we denote by $\hat{b}_{i_1}^{\mu_1}$ the visible biases in the zero-sum gauge. Following the pattern, we can write the expression for effective pairwise and fields for an arbitrary RBM:

$$\hat{J}_{i_1 i_2}^{\mu_1 \mu_2} = \frac{1}{q^{N_v}} \sum_{\mu'_1, \dots, \mu'_{N_v}} \sum_a \ln \frac{\left(1 + e^{c + W_{i_1 a}^{\mu_1} + W_{i_2 a}^{\mu_2} + \sum_{k=3}^{N_v} W_{i_k a}^{\mu'_k}} \right) \left(1 + e^{c + W_{i_1 a}^{\mu'_1} + W_{i_2 a}^{\mu'_2} + \sum_{k=3}^{N_v} W_{i_k a}^{\mu'_k}} \right)}{\left(1 + e^{c + W_{i_1 a}^{\mu_1} + W_{i_2 a}^{\mu'_2} + \sum_{k=3}^{N_v} W_{i_k a}^{\mu'_k}} \right) \left(1 + e^{c + W_{i_1 a}^{\mu'_1} + W_{i_2 a}^{\mu_2} + \sum_{k=3}^{N_v} W_{i_k a}^{\mu'_k}} \right)}, \tag{C9}$$

$$\hat{H}_{i_1}^{\mu_1} = \hat{b}_{i_1}^{\mu_1} + \frac{1}{q^{N_v}} \sum_{\mu'_1, \dots, \mu'_{N_v}} \sum_a \ln \left(\frac{1 + e^{c_a + W_{i_1 a}^{\mu_1} + W_{i_2 a}^{\mu'_2} + \sum_{k=3}^{N_v} W_{i_k a}^{\mu'_k}}}{1 + e^{c_a + W_{i_1 a}^{\mu'_1} + W_{i_2 a}^{\mu'_2} + \sum_{k=3}^{N_v} W_{i_k a}^{\mu'_k}}} \right). \tag{C10}$$

Moreover, we can further generalize the above considering an arbitrary n -th order coupling to obtain (10).

Appendix D: Gauge fixing of the multi-body Potts model

In the Refs. [15, 35], Feinauer et al. proved that Hamiltonians of energy-based models could be written as a Potts-like Hamiltonian with multi-body interactions in the zero-sum gauge. In [15], they also provided a closed expression for the corresponding effective pairwise couplings and fields, with a sampling estimator to compute them. Building upon that ground, in the following, we use what we have learned for the RBM case to establish a general mapping between probabilistic models and generalized Potts-like models, as they were defined in (6), with couplings given by (11). Hence, let us prove that this Potts-like formulation indeed keeps the probability mass distribution unchanged, which is equivalent to proof the following theorem:

Theorem 1. *Let π be a mass function defined over the sample space $\Omega \equiv \{1, 2, \dots, q\}^N$, such that $\pi(\mathbf{v}) > 0 \ \forall \mathbf{v} \in \Omega$, then $\pi(\mathbf{v}) \propto e^{-\mathcal{H}(\mathbf{v})}$ holds, considering the Hamiltonian definition:*

$$\begin{aligned}
\mathcal{H}(\mathbf{v}) &= - \sum_{n=1}^N \sum_{i_1=1}^{N-n+1} \sum_{i_2=i_1+1}^{N-n+2} \dots \sum_{i_n=i_{n-1}+1}^N \sum_{\mu_1=1}^q \dots \sum_{\mu_n=1}^q J_{i_1 \dots i_n}^{\mu_1 \dots \mu_n} \delta_{\mu_1}^{v_{i_1}} \dots \delta_{\mu_n}^{v_{i_n}} \\
&= - \sum_{n=1}^N \sum_{i_1=1}^{N-n+1} \sum_{i_2=i_1+1}^{N-n+2} \dots \sum_{i_n=i_{n-1}+1}^N \sum_{K \subseteq [n]} (-1)^{n-|K|} \mathbb{E}_{\mathbf{u} \sim G} [\ln \pi(\mathbf{u}) | u_{i_k} = v_{i_k} : k \in K]. \tag{D1}
\end{aligned}$$

Proof. Here, we will use a proof by *induction* in N . Let us choose $N=2$ as our *base case* for didactical reasons. When

$N = 2$, it is then straightforward to obtain that

$$\begin{aligned}\mathcal{H}(\mathbf{v}) &= -J_1^{v_1} - J_2^{v_2} - J_1^{v_1 v_2} \\ &= -(\mathbb{E}_{\mu \sim G} [\ln \pi(\mathbf{u}) | u_1 = v_1] - \mathbb{E}_{\mathbf{u} \sim G} [\ln \pi(\mathbf{u})]) - (\mathbb{E}_{\mathbf{u} \sim G} [\ln \pi(\mathbf{u}) | u_2 = v_2] - \mathbb{E}_{\mathbf{u} \sim G} [\ln \pi(\mathbf{u})]) \\ &\quad - (\mathbb{E}_{\mathbf{u} \sim G} [\ln \pi(\mathbf{u}) | u_1 = v_1, u_2 = v_2] - \mathbb{E}_{\mathbf{u} \sim G} [\ln \pi(\mathbf{u}) | u_1 = v_1] - \mathbb{E}_{\mathbf{u} \sim G} [\ln \pi(\mathbf{u}) | u_2 = v_2] + \mathbb{E}_{\mathbf{u} \sim G} [\ln \pi(\mathbf{u})]) \\ &= -\ln \pi(\mathbf{v}) + \mathbb{E}_{\mathbf{u} \sim G} [\ln \pi(\mathbf{u})].\end{aligned}\quad (\text{D2})$$

In the above we recognized that $\mathbb{E}_{\mathbf{u} \sim G} [\ln \pi(\mathbf{u}) | u_1 = v_1, u_2 = v_2] = \ln \pi(\mathbf{v})$, with $\mathbf{v} = (v_1, v_2)$. Since $\mathbb{E}_{\mathbf{u} \sim G} [\ln \pi(\mathbf{u})]$ is independent of \mathbf{u} (i.e., it is a constant), from the exponentiation of both sides of (D2) it follows that $\pi(\mathbf{v}) \propto e^{-\mathcal{H}(\mathbf{v})}$ holds for $N = 2$.

Next, assuming that the following identity holds for any probability mass π^* defined over a sample space Ω^* of dimension $N - 1$:

$$\begin{aligned}\mathcal{H}(\mathbf{v}^*) &= -\sum_{n=1}^{N-1} \sum_{i_1=1}^{N-n} \sum_{i_2=i_1+1}^{N-n+1} \dots \sum_{i_n=i_{n-1}+1}^{N-1} \sum_{K \subseteq [n]} (-1)^{n-|K|} \mathbb{E}_{\mathbf{u}^* \sim G^*} [\ln \pi^*(\mathbf{u}^*) | u_{i_k}^* = v_{i_k}^* : k \in K] \\ &= -\ln \pi^*(\mathbf{v}^*) + \mathbb{E}_{\mathbf{u}^* \sim G^*} [\ln \pi^*(\mathbf{u}^*)],\end{aligned}\quad (\text{D3})$$

we will prove that it also holds when the dimension of the sample space is N . First, Let us separate couplings that include the site $i_1 = 1$ from those that do not in (D1)

$$\begin{aligned}\mathcal{H}(\mathbf{v}) &= -\sum_{n=1}^N \sum_{i_1=1}^1 \sum_{i_2=2}^{N-n+2} \dots \sum_{i_n=i_{n-1}+1}^N \sum_{K \subseteq [n]} (-1)^{n-|K|} \mathbb{E}_{\mathbf{u} \sim G} [\ln \pi(\mathbf{u}) | u_{i_k} = v_{i_k} : k \in K] \\ &\quad - \sum_{n=1}^{N-1} \sum_{i_1=2}^{N-n+1} \sum_{i_2=i_1+1}^{N-n+2} \dots \sum_{i_n=i_{n-1}+1}^N \sum_{K \subseteq [n]} (-1)^{n-|K|} \mathbb{E}_{\mathbf{u} \sim G} [\ln \pi(\mathbf{u}) | u_{i_k} = v_{i_k} : k \in K].\end{aligned}\quad (\text{D4})$$

Besides, from coupling definition (11) we note that

$$\begin{aligned}J_{i_1 \dots i_n}^{\mu_1 \dots \mu_n} \delta_{\mu_1}^{v_{i_1}} \dots \delta_{\mu_n}^{v_{i_n}} &= \sum_{K \subseteq [n]} (-1)^{n-|K|} \mathbb{E}_{\mathbf{u} \sim G} [\ln \pi(\mathbf{u}) | u_{i_k} = v_{i_k} : k \in K] \\ &= \sum_{K \subseteq [n] \setminus \{1\}} (-1)^{n-|K|} \left[\mathbb{E}_{\mathbf{u} \sim G} [\ln \pi(\mathbf{u}) | u_{i_k} = v_{i_k} : k \in K] - \mathbb{E}_{\mathbf{u} \sim G} [\ln \pi(\mathbf{u}) | u_{i_k} = v_{i_k} : k \in K \cup \{1\}] \right].\end{aligned}\quad (\text{D5})$$

Replacing (D5) in the first line r.h.s. of (D4) line gives

$$\begin{aligned}&-\sum_{n=1}^N \sum_{i_1=1}^1 \sum_{i_2=2}^{N-n+2} \dots \sum_{i_n=i_{n-1}+1}^N \sum_{K \subseteq [n] \setminus \{1\}} (-1)^{n-|K|} \left[\mathbb{E}_{\mathbf{u} \sim G} [\ln \pi(\mathbf{u}) | u_{i_k} = v_{i_k} : k \in K] - \mathbb{E}_{\mathbf{u} \sim G} [\ln \pi(\mathbf{u}) | u_{i_k} = v_{i_k} : k \in K \cup \{1\}] \right] \\ &= \sum_{n=0}^{N-1} \sum_{i_1=2}^{N-n+1} \sum_{i_n=i_{n-1}+1}^N \sum_{K \subseteq [n]} (-1)^{n-|K|} \left[\mathbb{E}_{\mathbf{u} \sim G} [\ln \pi(\mathbf{u}) | u_{i_k} = v_{i_k} : k \in K] - \mathbb{E}_{\mathbf{u}^* \sim G^*} [\ln \pi(v_1, \mathbf{u}^*) | u_{i_k} = v_{i_k} : k \in K] \right],\end{aligned}\quad (\text{D6})$$

with $\mathbf{u}^* = (u_2, \dots, u_N)$, hence $\pi(v_1, \mathbf{u}^*) = \pi(v_1, \mu_2, \dots, \mu_N)$. Additionally, in (D6) we denoted by G^* the corresponding marginal probability mass function of G for $\mathbf{u}^* \in \Omega^*$. Substituting (D6) in (D4) gives

$$\begin{aligned}\mathcal{H}(\mathbf{v}) &= -\sum_{n=1}^{N-1} \sum_{i_1=2}^{N-n+1} \dots \sum_{i_n=i_{n-1}+1}^N \sum_{K \subseteq [n]} (-1)^{n-|K|} \mathbb{E}_{\mathbf{u}^* \sim G^*} [\ln \pi(v_1, \mathbf{u}^*) | u_{i_k}^* = v_{i_k} : k \in K] \\ &\quad + \mathbb{E}_{\mathbf{u} \sim G} [\ln \pi(\mathbf{u})] - \mathbb{E}_{\mathbf{u}^* \sim G^*} [\ln \pi(v_1, \mathbf{u}^*)]\end{aligned}\quad (\text{D7})$$

Using the induction hypothesis (D3) in (D7) lead us to verify that $\mathcal{H}(\mathbf{v}) = -\ln \pi(\mathbf{v}) + \mathbb{E}_{\mu \sim G} [\ln \pi(\mu)]$ holds. \blacksquare

In the above, we confirm that the probability distribution remains unchanged regardless of the G choice. This approach is advantageous because it allows us to gauge fix handily with the election of the distribution G over which

the average in (D1) is computed. For instance, let G be a degenerate distribution with probability mass function given by $g(\mathbf{u}) = \prod_{i=1}^N \delta_q^{v_i}$, from the coupling definition (11), with $\mu_n = q$, it follows that

$$\begin{aligned} J_{i_1 \dots i_n}^{\mu_1 \dots q} &= \sum_{K \subseteq [n]} (-1)^{n-|K|} \ln \pi(\mathbf{u} : u_{i_k} = \mu_k \text{ if } k \in K, u_l = q \text{ otherwise}) \\ &= \sum_{K \subseteq [n-1]} (-1)^{n-|K|} [\ln \pi(u_1, \dots, u_n : u_{i_k} = \mu_k \text{ if } k \in K, u_l = q \text{ otherwise}) \\ &\quad - \ln \pi(u_1, \dots, u_{n-1}, q : u_{i_k} = \mu_k \text{ if } k \in K, u_l = q \text{ otherwise})] = 0, \end{aligned} \quad (\text{D8})$$

which is the lattice gas gauge condition. Similarly, if G is the uniform distribution, one obtains

$$\begin{aligned} \sum_{\mu} J_{i_1 \dots i_n}^{\mu_1 \dots \mu} &= \sum_{K \subseteq [n-1]} (-1)^{n-|K|} \frac{1}{q^N} \sum_{\mu'_1, \dots, \mu'_N} \left[\ln \pi(u_1, \dots, u_n : u_{i_k} = \mu_k \text{ if } k \in K, u_l = \mu'_l \text{ otherwise}) \right. \\ &\quad \left. - \sum_{\mu} \ln \pi(u_1, \dots, u_{n-1}, \mu : u_{i_k} = \mu_k \text{ if } k \in K, u_l = \mu'_l \text{ otherwise}) \right] = 0, \end{aligned} \quad (\text{D9})$$

which is the zero-sum condition.
